

# Multi-period Power System Risk Minimization under Wildfire Disruptions

Hanbin Yang, Noah Rhodes, Haoxiang Yang, Line Roald, Lewis Ntaimo

**Abstract**—As climate change evolves, wildfire risk is increasing globally, posing a growing threat to power systems, with grid failures fueling the most destructive wildfires. In day-to-day operations, preemptive de-energization of equipment is an effective tool to mitigate the risk and damage of wildfires. However, such power outages have significant impacts on customers. This paper proposes a novel framework for planning preemptive de-energization of power systems to mitigate wildfire risk and damage. We model wildfire disruptions as stochastic disruptions with random magnitude and timing and formulate a two-stage stochastic program that maximizes the electricity delivered while proactively reducing the risk of wildfires by selectively de-energizing components over multiple time periods. We use cellular automata to sample grid failure and wildfire scenarios based on grid-related risks and environmental factors. We develop a decomposition algorithm that can generate adaptive shutoff plans before a disruption occurs. We test our method on an augmented version of the RTS-GLMC test case in Southern California and compare it with two benchmark cases. We find that our method reduces both wildfire damage costs and load-shedding losses over multiple time periods, and our nominal plan is robust against the uncertainty model perturbation.

**Index Terms**—optimal power flow, stochastic mixed-integer programming, wildfire risk, de-energization, Lagrangian cut, decomposition algorithm.

## I. INTRODUCTION

In recent years, wildfire-related disasters have become more frequent and severe across the United States [1], [2]. More than 32,000 wildfires happened between 2011 and 2013 and destroyed about 5,800 buildings in Texas. Many catastrophic fires with significant loss of life and property were sparked by electric power infrastructures [3]. The Camp Fire in 2018, sparked by a transmission line, claimed 84 lives and caused an estimated \$9.3 billion in damage to the residential property alone [4]. Administrative investments in wildfire suppression alone are not enough to mitigate wildfire risks, and it requires new studies to examine the interaction between power system operations and wildfire management [5].

We classify wildfires into two categories, *exogenous* and *endogenous* fires, as they interact with power systems differently: exogenous fires are external to the power system, while endogenous fires are triggered by power system faults. Exogenous wildfires can be caused by extreme weather conditions such as drought conditions [6], and they spread faster under windy conditions. The power system equipment may be damaged when it comes into contact with exogenous wildfires. On the other hand, endogenous fires are ignited when downed transmission lines get in contact with surrounding vegetation and can also damage nearby power system components [7].

A framework to assess wildfire risk is proposed [8], and such wildfire simulation models can provide early warnings [9].

Approaches to reduce the risk of wildfire ignitions and their adaptation is being considered by utilities. Long-term approaches can last for years, such as regular equipment inspection, frequent vegetation management, and protection system installation [10]. For example, Pacific Gas and Electric (PG&E) has announced a plan to install underground 10,000 miles of distribution lines, at the cost of \$20 billion over 10 years, while taking other precautions such as revegetating the areas along transmission lines more frequently [11]. Such a long-term plan, although important, often requires enormous costs and qualified personnel and equipment and should be complemented with day-to-day operations such as de-energizing power lines during extreme weather to eliminate risk. De-energized lines will not fault and spark wildfires but may cause intentional blackouts, referred to as public power safety shut-offs (PSPS) [12]. If not executed properly, such de-energization can have an enormous and long-lasting impact on the economy and society [13].

There is an urgent need for optimization under uncertainty applied to power system de-energization strategies under wildfire risk [14]. Many of the existing studies focus on deterministic wildfire risk models, such as a wildfire hazard prevention system based on data mining techniques [15], a deterministic optimization model for the trade-off between wildfire risk and load shedding [7], and a data-driven wildfire decision-making framework for power system resilience [16]. While more models have started to incorporate stochastic aspects of wildfire risks recently, such as a dynamic programming model to optimize a PSPS [17] and a rolling horizon optimization problem for joint de-energization and restoration [18], most of the literature still focus on the exogenous fire hazard with a relatively simple decision structure. Optimizing a sequential decision process that models both the shut-off and power flow decisions requires solving a multistage stochastic program. This can be challenging because the computational complexity increases exponentially with the planning horizon length [19] and there may be integer variables involved [7].

We develop a two-stage stochastic mixed-integer programming (SMIP) model that captures the interaction between power system de-energization and both exogenous and endogenous wildfire risks over multiple periods. In addition, our two-stage SMIP model incorporates the spatial and temporal uncertainty of wildfires and represents real-world situations with disruption scenarios, which can handle complex and dynamic situations better and produce more resilient operations than deterministic models. We use cellular automata

to simulate wildfire spread and generate scenarios that describe the magnitude and timing of wildfire disruptions. Since wildfire occurs infrequently, we assume at most one wildfire occurrence during the planning horizon to reduce the multi-period problem into two stages [20]. We design a proactive de-energization scheme that executes an effective protection plan before the wildfire and optimizes the power flow operations of the remaining available components after the disruption.

We propose a decomposition algorithm for SMIP with non-convex and non-smooth value functions. Our algorithm uses linear cutting planes, named *Lagrangian cuts*, to approximate the value functions [21]. Lagrangian cuts are tight at any binary incumbent solution but can be inefficient when the master problem has many sub-optimal solutions and the sub-problems are complicated. To overcome this limitation, we introduce an enhanced version of the Lagrangian cut, named *square-minimization cut*, which improves the quality of the approximations and speeds up the algorithm. Our method shows high computational accuracy and reliability. The two-stage SMIP model supports the decision-making process under uncertainty, reduces the likelihood of a disaster, and maintains as much load delivery as possible after a disruption.

The contributions of our paper are fourfold:

i) We propose a cellular automaton model that simulates the onset and spread of both exogenous and endogenous wildfires based on environmental data. This enables us to assess wildfire risk through scenarios used in the SMIP model.

ii) We formulate a two-stage SMIP model that manages wildfire risk in power system operations. Unlike the existing literature, our model captures the random nature of wildfire ignitions using disruption scenarios with random onset times to keep the model size manageable.

iii) We develop a cutting plane algorithm that solves the SMIP model with finite convergence. We improve its computational performance with a new square-minimization cut.

iv) We show our two-stage SMIP model yields significantly more resilient solutions, compared to its deterministic benchmarks on the RTS-GLMC test case, and analyze the solution under different parametric settings to gain operational insights.

The rest of the paper is organized as follows: Section II presents the wildfire simulation model and the SMIP formulation; Section III derives the cutting plane algorithm and its computational enhancement; Section IV covers benchmark cases and numerical analyses; and Section V concludes the paper with a brief discussion of future work.

## II. TWO-STAGE SMIP MODEL

### NOMENCLATURE

#### Indices and index sets

$\mathcal{B}$	set of buses;
$\mathcal{G}$	set of generators;
$\mathcal{L}$	set of transmission lines;
$\mathcal{D}$	set of load demand;
$\mathcal{C}$	set of load components, $\mathcal{C} = \mathcal{B} \cup \mathcal{G} \cup \mathcal{L}$ ;
$\mathcal{T}$	set of time periods, $\mathcal{T} = \{1, 2, \dots, T\}$ ;
$\Omega$	index set of wildfire scenarios;
$I_c^\omega$	set of affected components by component $c$ 's ignition under scenario $\omega \in \Omega$ ;

#### Parameters

$D_{dt}$	load $d \in \mathcal{D}$ at time period $t \in \mathcal{T}$ ;
$w_d$	the priority level of load $d \in \mathcal{D}$ ;
$r_c$	repair cost for component $c \in \mathcal{C}$ ;
$\underline{P}_g^G, \bar{P}_g^G$	maximum and minimum generation limits of $g \in \mathcal{G}$ ;
$\bar{W}_{ij}$	the thermal power flow limit of the line $(i, j) \in \mathcal{L}$ ;
$b_{ij}$	the susceptance of the line $(i, j) \in \mathcal{L}$ ;
$\theta, \bar{\theta}$	the big-M values for voltage angle difference;
$\tau^\omega$	disruption time for scenario $\omega \in \Omega$ ;
$u_c^\omega$	1 if component $c \in \mathcal{C}$ faults under scenario $\omega \in \Omega$ , 0 otherwise;
$v_c^\omega$	1 if component $c \in \mathcal{C}$ is shut off by exogenous fire under scenario $\omega \in \Omega$ , 0 otherwise;

#### Decision variables

$\theta_{it}$	phase angle of the bus $i \in \mathcal{B}$ at time $t \in \mathcal{T}$ ;
$P_{ijt}^L$	active power flow on the line $(i, j) \in \mathcal{L}$ at time $t \in \mathcal{T}$ ;
$p_{gt}^G$	active power generation at generator $g \in \mathcal{G}$ at time $t \in \mathcal{T}$ ;
$x_{dt}$	percentage of demand satisfied at the load $d \in \mathcal{D}$ at time $t \in \mathcal{T}$ ;
$z_{ct}$	1 if component $c \in \mathcal{C}$ is functional at time $t \in \mathcal{T}$ , 0 otherwise;
$y_{ct}^\omega$	1 if component $c \in \mathcal{C}$ is functional at time $t \in \mathcal{T}$ under scenarios $\omega \in \Omega$ , 0 otherwise;
$\nu_{ct}^\omega$	1 if a fire damage is incurred at component $c \in \mathcal{C}$ at time $t \in \mathcal{T}$ under scenarios $\omega \in \Omega$ , 0 otherwise.

We consider multi-period dispatch and de-energization operations under wildfire disruption over a short-term time horizon (24 hours). The power network is represented by a graph  $(\mathcal{B}, \mathcal{L})$ , where  $\mathcal{B}$  is the set of buses and  $\mathcal{L}$  is the set of lines. We use  $\mathcal{D}_i$ ,  $\mathcal{G}_i$ , and  $\mathcal{L}_i$  to represent the subset of loads, generators, and transmission lines connected to bus  $i$ , respectively. For each period  $t \in \mathcal{T}$ , we formulate DC power flow constraints to decide the active power generation  $P_{gt}^G$  of generator  $g \in \mathcal{G}$ , the power flow  $P_{ijt}^L$  on transmission line  $(i, j) \in \mathcal{L}$  from bus  $i$  to bus  $j$ , and the phase angle  $\theta_{it}$  of bus  $i \in \mathcal{B}$ .

#### A. Wildfire Scenario Modeling

On top of the constructed electric power network, we model wildfire uncertainty as a stochastic disruption with random occurrence timing, location, and spread. We consider a short-term operation and thus assume at most one disruption will occur over the time horizon. We form a portfolio of disruption scenarios indexed by  $\omega \in \Omega$ , within which we model i) endogenous fires, which are caused by faults of operating electric components, and ii) exogenous fires, which are caused by random natural wildfire ignitions.

We consider the smallest rectangular area that can cover the entire power network and divide it into a two-dimensional grid of a specified resolution, in which the set of cells is denoted by  $\mathcal{K}$ . We then construct a mapping between the grid cells and the buses and transmission lines based on their geographic locations. We let  $k_i \in \mathcal{K}$  denote the cell where the bus  $i$  is located. A transmission line,  $l = (i, j)$ , can span multiple cells, which is denoted by  $\mathcal{K}_{ij}$ . Furthermore, a cell  $k \in \mathcal{K}$  can contain multiple transmission lines, and we denote the set of transmission lines passing cell  $k$  by  $\mathcal{L}^k$ . Finally, we let  $\mathcal{K}_B$

and  $\mathcal{K}_{\mathcal{L}}$  be the collection of cells containing at least a bus and at least a transmission line, respectively.

We employ the cellular automata method, with propagation rules listed in [22], to simulate the spread of exogenous wildfires. Each cell is characterized by four states which evolve in discrete time. The four states are as follows: (i) *cell has no forest fuel*; (ii) *cell has forest fuel that has not ignited*; (iii) *cell has ignited forest fuel*; (iv) *cell has fully burning forest fuel*. Endogenous disruptions are caused by power system component failures. The status of each component is normal, at fault, or ignited. We define the onset time of a wildfire disruption  $\tau^\omega$  as the earlier time between an exogenous wildfire occurrence and any electric component's fault.

a) *Exogenous Wildfires*: We assume that there are no exogenous wildfires in the grid at the start of the time horizon. For each cell  $k \in \mathcal{K}$  in period  $t \in \mathcal{T}$ , it receives information from the environment to update its state and interacts with surrounding cells: if its state in period  $t - 1$  is (ii) (unburned fuel), it has a probability  $p_{tk}$ , influenced by environmental factors, to be ignited and its state will transfer from (ii) to (iii) (ignited fuel); if its state in period  $t - 1$  is (iii), then the state will transfer to (iv) (fully burning); if it is a fully burning cell, the state will stay at (iv) and can spread flames to its 8 adjacent cells indexed by  $k'$ , igniting them with probabilities  $q_{tk'}$  if they are in status (ii), where parameters  $q_{tk'}$  are subject to environmental factors like vegetation, ground elevation, and wind. We record the exogenous wildfire damage after the end of time horizon  $\mathcal{T}$ , letting  $v_c^\omega = 1$  if a wildfire (state (iii) or (iv)) ever occurs on  $k_i$  if  $c$  is bus  $i$  or any generator connected to bus  $i$ , or on any cell in  $\mathcal{K}_{ij}$ , if  $c$  is transmission line  $(i, j)$ .

b) *Endogenous Wildfires*: We simulate endogenous wildfires using a two-step procedure. First, we simulate electrical component faults. To initialize the fault simulation process, we assume there is no fault component in the power system at the start of the time horizon, similar to the exogenous wildfire simulation. For every period  $t \in \mathcal{T}$ , a fault may occur at a component  $c \in \mathcal{C}$  following a Bernoulli distribution with probability  $p_{tc}$ . Once a component faults, we record the state by letting  $u_c^\omega = 1$ . Our second step runs an independent cellular automaton process for each fault component  $c$  from the fault period to the end of the time horizon, initialized with the cell(s) that contains the component in state (iii). After the cell evolves to state (iv) in the next period, it will spread the simulated wildfire to the adjacent cell  $k'$  with a probability  $q_{t,k'}$  at time period  $t$  and further propagate. The components damaged by this spread in the time horizon form a set  $I_c^\omega$ . Fig. 1 gives an illustration of such a set. Notice that we assume a fault directly leads to a wildfire because we aim to simulate how an endogenous fire would spread if the component  $c$  were not de-energized. In addition, we build independent simulation processes, each starting with only the cell(s) containing the fault component  $c$ , in order to clearly trace the spread of a wildfire to its origin and eliminate the interference of endogenous wildfires started elsewhere.

In summary, for a specific scenario  $\omega \in \Omega$ , we use cellular automata procedures to generate the wildfire disruption uncertainty  $\xi^\omega = \{\tau^\omega, v_c^\omega, u_c^\omega, I_c^\omega\}$ , which includes the disruption time  $\tau^\omega$ , the binary parameters  $v_c^\omega$  indicating the exogenous

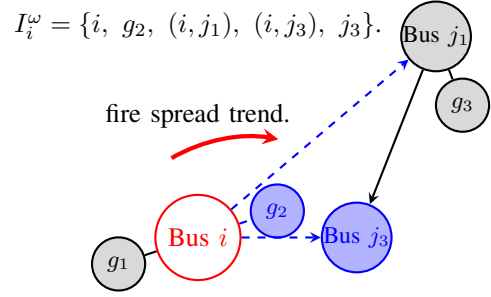


Fig. 1: A random set  $I_i^\omega$  illustration. Bus  $i$  faults in this scenario, resulting in a fire that spreads and affects two transmission lines, bus  $j_3$ , and generator  $g_2$ .

fire locations, the binary parameters  $u_c^\omega$  indicating the fault locations, and the set  $I_c^\omega$  characterizing components damaged by the potential endogenous fire at component  $c$ .

### B. Two-Stage SMIP Model

When a fault occurs at an energized component, the associated endogenous wildfire may incur high damage costs. To reduce the endogenous risk of igniting a wildfire, the power system operator can de-energize, i.e., shut off, power equipment. However, suppose multiple components are de-energized to prevent endogenous fires. In that case, the power supply capacity may be greatly reduced, resulting in the inability to meet crucial load demand and causing serious secondary disasters. To improve the reliability of the power system and mitigate wildfire damage, operators should de-energize some potentially dangerous electrical equipment under high-risk conditions to ensure enough power supply while significantly reducing risk.

To balance the risk trade-off between endogenous fire and load shedding, we build a two-stage SMIP model (1) which optimizes shut-off decisions under wildfire disruption uncertainty over the given time horizon. In model (1), a de-energized generator will have zero generation capacity, and a de-energized line will be considered open. If a bus is shut off, all generators and lines connected to it will also be de-energized. Our model uses binary decision variables  $z_{ct}$  to represent whether a component  $c \in \mathcal{C}$  is de-energized at time period  $t$ . We assume that a de-energized component will remain off until the end of the time horizon due to safety considerations [7]. Model (1) obtains a first-stage plan, i.e., a nominal plan, that should be implemented until a disruption occurs or the time horizon ends, whichever occurs first. If a fire disruption is observed at period  $\tau^\omega$ , given the current shut-off state  $z_{\tau^\omega-1}$ , the model enters the second stage and incurs the second-stage value function  $f^\omega$ , where we assume that the components at revealed ignition locations will be shut off.

$$Z^* = \min \sum_{\omega \in \Omega} p^\omega \left[ \sum_{t=1}^{\tau^\omega-1} \sum_{d \in \mathcal{D}} w_d (1 - x_{dt}) + f^\omega(z_{\tau^\omega-1}, \xi^\omega) \right]$$

s.t.  $\forall t \in \mathcal{T}$ :

$$P_{ijt}^L \leq -b_{ij} (\theta_{it} - \theta_{jt} + \bar{\theta}(1 - z_{ijt})) \quad \forall (i, j) \in \mathcal{L} \quad (1a)$$

$$P_{ijt}^L \geq -b_{ij} (\theta_{it} - \theta_{jt} + \underline{\theta}(1 - z_{ijt})) \quad \forall (i, j) \in \mathcal{L} \quad (1b)$$

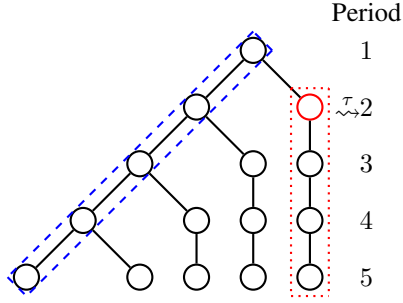


Fig. 2: A scenario-tree illustration of the wildfire disruption problem with  $T = 5$  and  $\tau^\omega = \tau = 2$ .

$$-W_{ij}z_{ijt} \leq P_{ijt}^L \leq W_{ij}z_{ijt} \quad \forall (i, j) \in \mathcal{L} \quad (1c)$$

$$\sum_{g \in \mathcal{G}_i} P_{gt}^G + \sum_{(i,j) \in \mathcal{L}_i} P_{ijt}^L = \sum_{d \in \mathcal{D}_i} D_{dt}x_{dt} \quad \forall i \in \mathcal{B} \quad (1d)$$

$$P_g^G z_{gt} \leq P_{gt}^G \leq \bar{P}_g^G z_{gt} \quad \forall g \in \mathcal{G} \quad (1e)$$

$$z_{it} \geq x_{dt} \quad \forall i \in \mathcal{B}, d \in \mathcal{D}_i \quad (1f)$$

$$z_{it} \geq z_{gt} \quad \forall i \in \mathcal{B}, g \in \mathcal{G}_i \quad (1g)$$

$$z_{it} \geq z_{ijt} \quad \forall i \in \mathcal{B}, (i, j) \in \mathcal{L} \quad (1h)$$

$$z_{it} \geq z_{jit} \quad \forall i \in \mathcal{B}, (j, i) \in \mathcal{L} \quad (1i)$$

$$z_{ct} \geq z_{c \min\{t+1, T\}} \quad \forall c \in \mathcal{C} \quad (1j)$$

$$z_{ct} \in \{0, 1\} \quad \forall c \in \mathcal{C}. \quad (1k)$$

The objective function considers the expected cost, which consists of the load-shedding cost before the disruption and the total cost after the disruption. Constraints (1a)-(1e) correspond to the DC power flow model and constraints (1f)-(1i) model the component interactions, equivalent to constraint (7)-(9) in [7]. Constraints (1j) describe the temporal logic of components' status: once a component is shut off, it stays off, and the corresponding  $z$  variable is 0. The scenario tree of this two-stage SMIP model is shown as Fig. 2, in which each node represents the decisions at a time period, and each branch extending to the right represents a disruption scenario. The blue box of the left diagonal branch represents the nominal plan obtained if no disruption occurs. Suppose we have a scenario  $\omega$  with  $\tau^\omega = 2$ . The red box on the right describes the decisions associated with such value function  $f^\omega$ .

The second-stage value function  $f^\omega$  takes in the shut-off state variables  $\hat{z}_{c\tau^\omega-1}$  and the disruption uncertainty  $\xi^\omega$  as its input. It focuses on the operations after  $\tau^\omega$  and can be evaluated by solving the following mixed-integer program:

$$\min \sum_{t=\tau^\omega}^T \sum_{d \in \mathcal{D}} w_d(1 - x_{dt}^\omega) + \sum_{c \in \mathcal{C}} r_c \nu_c^\omega$$

$$\text{s.t. } \forall t \in \{\tau^\omega, \dots, T\}:$$

$$P_{ijt}^{L,\omega} \leq -b_{ij}(\theta_{it}^\omega - \theta_{jt}^\omega + \bar{\theta}(1 - y_{ij}^\omega)) \quad \forall (i, j) \in \mathcal{L} \quad (2a)$$

$$P_{ijt}^{L,\omega} \geq -b_{ij}(\theta_{it}^\omega - \theta_{jt}^\omega + \bar{\theta}(1 - y_{ij}^\omega)) \quad \forall (i, j) \in \mathcal{L} \quad (2b)$$

$$-W_{ij}y_{ijt}^\omega \leq P_{ijt}^{L,\omega} \leq W_{ij}y_{ijt}^\omega \quad \forall (i, j) \in \mathcal{L} \quad (2c)$$

$$\sum_{g \in \mathcal{G}_i} P_{gt}^{G,\omega} + \sum_{(i,j) \in \mathcal{L}_i} P_{ijt}^{L,\omega} = \sum_{d \in \mathcal{D}_i} D_{dt}x_{dt}^\omega \quad \forall i \in \mathcal{B} \quad (2d)$$

$$P_g^{G,\omega} y_g^\omega \leq P_{gt}^{G,\omega} \leq \bar{P}_g^{G,\omega} y_g^\omega \quad \forall g \in \mathcal{G} \quad (2e)$$

$$y_i^\omega \geq x_{dt}^\omega \quad \forall i \in \mathcal{B}, d \in \mathcal{D}_i \quad (2f)$$

$$y_i^\omega \geq y_g^\omega \quad \forall i \in \mathcal{B}, g \in \mathcal{G}_i \quad (2g)$$

$$y_i^\omega \geq y_{ij}^\omega \quad \forall i \in \mathcal{B}, (i, j) \in \mathcal{L} \quad (2h)$$

$$y_i^\omega \geq y_{ji}^\omega \quad \forall i \in \mathcal{B}, (j, i) \in \mathcal{L} \quad (2i)$$

$$y_c^\omega \leq z_c^\omega \quad \forall c \in \mathcal{C} \quad (2j)$$

$$y_c^\omega \leq 1 - \nu_c^\omega \quad \forall c \in \mathcal{C} \quad (2k)$$

$$\nu_c^\omega \geq v_c^\omega \quad \forall c \in \mathcal{C} \quad (2l)$$

$$\nu_k^\omega \geq u_c^\omega z_c^\omega \quad \forall c \in \mathcal{C}, k \in I_c^\omega \quad (2m)$$

$$z_c^\omega = \hat{z}_{c\tau^\omega-1} \quad \forall c \in \mathcal{C} \quad (2n)$$

$$y_c^\omega, \nu_c^\omega, z_c^\omega \in \{0, 1\} \quad \forall c \in \mathcal{C}. \quad (2o)$$

The objective function includes the load-shedding cost after the disruption and the wildfire damage cost. The wildfire damage cost for a component  $c \in \mathcal{C}$ , denoted by  $r_c$ , consists of the replacement cost of the electric components and the financial loss to the nearby communities. In model (2), the energization status will stay the same in the remaining time horizon, as we assume that all wildfire damages reveal at period  $\tau^\omega$  and no recovery decisions take place afterward. Constraints (2a)-(2e) model an equivalent form of the DC power flow constraints as in model (1). Constraints (2f)-(2i) indicate the functioning state of components, similar to their first-stage counterparts (1f)-(1i). We create a local copy of the first-stage shut-off decisions,  $z_c^\omega$ , via the duplicating constraint (2n), which is known as the nonanticipativity constraint. With  $z_c^\omega$  indicating whether component  $c$  has been shut off, constraint (2j) makes sure that the shut-off components stay down through the second stage. Constraint (2k) states that damaged components no longer function, where we model the exogenous fire damage by constraint (2l) and the endogenous fire damage by constraint (2m). Notice that an endogenous fire started at component  $c$  requires both a fault occurrence  $u_c^\omega = 1$  and the component not being shut off  $z_c^\omega = 1$  and spreads to components  $k \in I_c^\omega$ .

### III. DECOMPOSITION ALGORITHM BASED ON LAGRANGIAN CUT

The value function  $f^\omega$  is a non-convex function without an analytical form, as we need to solve a MIP subproblem (2) to evaluate it. A common way to solve model (1) is to replace  $f^\omega$  with closed-form approximation, such as linear cutting planes. If the state variables are binary, we can generate Lagrangian cuts to equivalently reformulate  $f^\omega$  as a convex piecewise linear function [21]. Such Lagrangian cuts can be applied to model (1) as well because our state variables  $z$  are binary. In this section, we first show the derivation of the Lagrangian cut and the convergence properties of the cutting plane method. In addition, we propose an improved Lagrangian cut, *square-minimization cut* (SMC), and illustrate how it can accelerate the cutting plane algorithm.

At  $\ell$ -th iteration, we solve a Lagrangian dual problem (3) to obtain the cut intercept  $v^{\omega,\ell}$  as its optimal value  $v^*$  and gradient  $\lambda^{\omega,\ell}$  as the optimal solution  $\lambda^*$ . Notice that model (3) is a convex program and can be solved via convex programming algorithms such as the level-set methods in [23].

$$v^* = \max_{\lambda} R(\hat{z}, \lambda), \quad (3)$$

where the Lagrangian relaxation problem  $R(\hat{z}, \lambda)$  is obtained by relaxing the nonanticipativity constraint (2n):

$$R^\omega(\hat{z}, \lambda) = \min \sum_{t=\tau^\omega}^T \sum_{d \in \mathcal{D}} w_d(1 - x_{dt}) + \sum_{c \in \mathcal{C}} [r_c v_c^\omega + \lambda_c(\hat{z}_{c, \tau^\omega-1} - z_c^\omega)] \quad (4)$$

s.t. Constraints (2a) – (2m).

Since we can always find a feasible solution to subproblem (2) by setting all variables in model (2) to zero, we do not need to generate feasibility cuts to characterize the domain of  $f^\omega$  and can focus on generating optimality cuts to approximate  $f^\omega$  [19]. For a specific  $\omega$ , we denote the lower approximation of  $f^\omega$  by  $V^\omega$ , and write the  $\ell$ -th cut as follows:

$$V^\omega \geq v^{\omega, \ell} + (\lambda^{\omega, \ell})^\top (z_{\tau^\omega-1} - \hat{z}_{\tau^\omega-1}^\ell). \quad (5)$$

With construction of  $L$  Lagrangian cuts (5), we can substitute the function  $f^\omega$  by  $V^\omega$  to obtain the lower approximation for model (1) as  $(M_L)$ . Since the cuts form a lower approximation of  $f^\omega$ , the optimal value  $Z_L^*$  is a lower bound of  $Z^*$ .

$$(M_L) \quad Z_L^* = \min \sum_{\omega \in \Omega} p_t^\omega \left[ \sum_{t=1}^{\tau^\omega-1} w_d(1 - x_{dt}) + V^\omega \right] \quad (6)$$

s.t. Constraints (1a) – (1j)

$$V^\omega \geq (\lambda^{\omega, \ell})^\top (z_{\tau^\omega-1} - \hat{z}_{\tau^\omega-1}^\ell) + v^{\omega, \ell}, \quad \forall \omega \in \Omega, \ell = 1, \dots, L.$$

Once we obtain the optimal solution  $(\hat{x}, \hat{z}, \hat{\theta}, \hat{P})$  to  $(M_L)$ , it is a feasible solution to model (1) and we can calculate an upper bound by evaluating  $f^\omega(\hat{z}_{\tau^\omega-1}, \xi^\omega)$  for each  $\omega \in \Omega$ . We present the detailed steps of the decomposition algorithm in Algorithm 1 below, which iteratively updates the bounds. In the end, we terminate Algorithm 1 once the relative gap is within a predefined tolerance threshold  $\epsilon \geq 0$ . We can show that Algorithm 1 converges to the optimal value in finite steps.

**Theorem 1 (Convergence).** *When  $\epsilon = 0$ , Algorithm 1 terminates in a finite number of iterations and outputs an optimal solution to model (1) after finitely many iterations  $L$ .*

*Proof.* By Theorem 3 in [21], the Lagrangian cut is a tight evaluation for the value function at the given incumbent first-stage solution because of the binary state variables  $\hat{z}$ . Since the cuts can precisely represent the values of  $f^\omega$  at any given first-stage solutions and there are finitely many first-stage solutions  $z$ , we can fully describe the value function after finitely many cuts. Hence, there exists a finite number of iterations,  $k_1$ , beyond which no new cuts are generated. From iteration  $k_1$  onwards, we can then apply Theorem 2 in [21] to establish that Algorithm 1 terminates with an optimal solution in finite steps when  $\epsilon = 0$ .  $\square$

Although the Lagrangian cut (5) is tight and valid at the incumbent binary solution  $\hat{z}$  and results in finite convergence, the cut may be steep and not provide a good lower approximation at other solutions (shown as the black line in Fig. 3). Therefore, We propose a rotated cut, the SMC, which is illustrated by the

---

**Algorithm 1:** Decomposition algorithm based on Lagrangian cuts to solve model (1)

---

```

1 Initialization cut iteration number  $\ell = 0$ , lower bound
    $LB = 0$ , upper bound  $UB = \infty$  and  $\epsilon \geq 0$ ;
2 while  $\frac{UB-LB}{UB} \geq \epsilon$  do
   /* Forward Steps */
3   Solve the master problem  $(M_\ell)$  and obtain the first-stage
   shut-off solution  $\hat{z}^\ell$ , optimal value  $Z_\ell^*$ , and the
   approximations of value function  $\hat{\theta}^{\omega, \ell}$ ;
4   Update  $LB = Z_\ell^*$ ;
5   for  $\omega \in \Omega$  do
6     Solve model (2) with  $\hat{z}^\ell$  and obtain  $f^\omega(\hat{z}_{\tau^\omega}^\ell, \xi^\omega)$ ;
7   end
8   Let  $\bar{Z} = Z_\ell^* + \sum_{\omega \in \Omega} p^\omega (f^\omega(\hat{z}_{\tau^\omega}^\ell, \xi^\omega) - \hat{\theta}^{\omega, \ell})$ ;
9   if  $\bar{Z} < UB$  then
10    Update  $UB = \bar{Z}$  and incumbent solution as
         $z^* = \hat{z}^\ell$ ;
11  end
   /* Backward Steps */
12  for  $\omega \in \Omega$  do
13    Solve the Lagrangian dual problem (3), and obtain
        the optimal solution  $\lambda^{\omega, \ell}$  and the optimal value
         $v^{\omega, \ell} = R^\omega(\hat{z}^\ell, \lambda^{\omega, \ell})$ ;
14    And add cut (5) to  $(M_\ell)$ ;
15  end
16  Let  $\ell = \ell + 1$ ;
17 end
18 Output the  $\epsilon$ -optimal value  $UB$  and solution  $z^*$ .
```

---

red line in Fig. 3. Instead of solving model (3) to obtain the cut coefficients  $\lambda$  and  $v$ , we solve an alternative model:

$$\min_{\lambda} \lambda^\top \lambda \quad (7a)$$

$$\text{s.t. } R^\omega(\hat{z}, \lambda) \geq (1 - \delta) f^\omega(\hat{z}_{\tau^\omega-1}, \xi^\omega), \quad (7b)$$

and we let  $\lambda^{\omega, \ell}$  equal to its optimal solution  $\lambda^*$  and  $v^{\omega, \ell} = R^\omega(\hat{z}, \lambda^*)$ . Fig. 3 shows that the difference between a steep cut and a flat cut lies in the angle they make with the horizontal plane. We prefer a flat cut, corresponding to a smaller  $\lambda^\top \lambda$ , as  $\lambda$  represents the linear cut's coefficients. While we minimize  $\lambda^\top \lambda$  and rotate the cut, it is possible that the cut becomes non-tight at the incumbent solution  $\hat{z}$ . Therefore, we set up constraint (7b) to force the cut value to be within a  $\delta$  neighborhood of  $f^\omega$  at  $\hat{z}$ , which can be considered an ‘‘anchor point.’’ Model (7) is always feasible as the Lagrangian cut coefficients obtained from solving model (3) can serve as a feasible solution, and we can use similar convex programming solution methods to solve model (7).

#### IV. NUMERICAL RESULTS

In this section, we first describe the numerical experiment setup, with which we evaluate the efficiency of our decomposition method and the solution quality. We then compare our two-stage SMIP model (1) with three benchmark cases: a deterministic model that ignores wildfire disruption, a wait-and-see model with perfect wildfire information, and a model based on an aggregate wildfire risk metric. Finally, we examine the robustness of our nominal solution against potential inaccuracy in wildfire disruption probability.

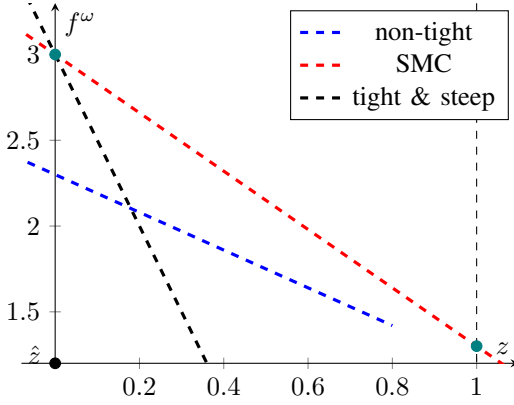


Fig. 3: Illustration of different types of cuts: the black cut and the red cut are tight at  $\hat{z} = 0$ , but the blue cut is not since its value at  $\hat{z}$  is smaller than the function value; the red cut has better performance than the black cut as it also characterizes the function value exactly at another  $\hat{z} = 1$ .

#### A. Experiment Setup

We use the RTS-GMLC 73-bus case [24] and run experiments on a 24-hour horizon with each time period accounting for an hour ( $T = 24$ ). We assume a constant electricity demand except for the peak hours, 9 am to 12 pm and 3 pm to 7 pm, during which the demand is 1.2 times the non-peak value.

The economic loss caused by fire and sudden power outages depends on the fire intensity and the amount of load in the affected area. To quantify the economic impact of wildfire damage and load loss, we assign each electrical component a numerical rating based on its importance and impact on the area, following a similar approach to the *Value Response Index* in Texas Wildfire Risk Rating System [25]. To make the values comparable, we scaled the data from [26], [27], [28], and [29] to obtain the following cost parameters:

- 1) Load priorities  $w_d$  range from 50 to 1000;
- 2) The damage costs  $r_c$  of wind turbines, thermal and nuclear power plants are 50, 1000, and 2500, respectively;
- 3) The damage cost  $r_c$  of each bus is 50;
- 4) The damage cost  $r_c$  of a transmission line is  $0.285\ell$ , where  $\ell$  is the length of the transmission line.

Fig. 4 color codes the load and generator priority levels based on their load-shedding and damage costs, respectively.

All optimization models were implemented using JuMP [30] in Julia v1.6 [31] and solved by Gurobi v9.5.1 [32] on a computer with a 10-core M1 Pro CPU and 32GB memory. The network plots are generated using PowerPlot.jl, which depends on PowerModels.jl package [33]. Scenario simulation is constructed by an agent-based model package, Agent.jl [34]. For Algorithm 1 and SMC, we set  $\epsilon = 1\%$  and  $\delta = 10^{-4}$ .

#### B. Scenario Setup

In this section, we detail the parameter setup used in the simulation process of Section II-A. Overall, this setup leads to a wildfire disruption in approximately 95% of scenarios.

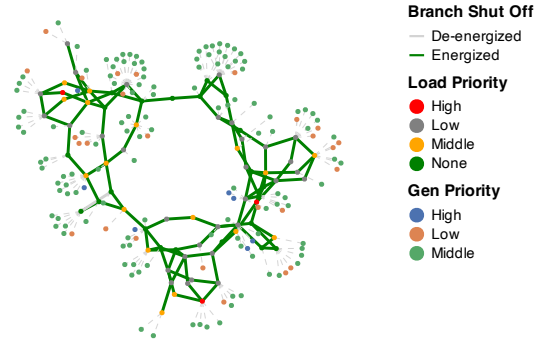


Fig. 4: Illustration of the RTS-GMLC system.

*Mapping onto Grid:* We convert the location of each bus  $i \in \mathcal{B}$  from latitude and longitude [24] to Universal Transverse Mercator (UTM) coordinates [35]. The smallest rectangle that contains the entire power network has a length of 180,000 and a width of 138,000 UTM unit. We divide such a rectangular area into square cells with an edge length of 1,000 UTM units.

*Probability of Exogenous Wildfire Ignition  $p_{tk}$ :* We assume that only wildfires that occur in cells with at least one power system component will threaten the electric power system. As stated in Section II-A, we model the ignition of exogenous wildfires at time  $t$  by a probability  $p_{tk}$ , which describes the likelihood of a cell  $k \in \mathcal{K}$  transitioning from the state (ii), un-burned fuel, to state (iii), ignited the fuel. To estimate  $p_{tk}$ , we use the Wildland Fire Potential Index (WFPI) [36] as a measure of the relative probability of ignition. The probability of an exogenous wildfire occurring in cell  $k$  in which the set of all transmission lines passing through cell  $k$  is  $\mathcal{L}^k$  is

$$p_{tk} = \frac{\sum_{l \in \mathcal{L}^k} \text{WFPI}_l}{\sum_{l' \in \mathcal{L}} \text{WFPI}_{l'}}.$$

*Probability of Wildfire Spread  $q_{tk'}$ :* Suppose there is a fully burning cell. Each of the adjacent cells  $k' \in \mathcal{K}$  will be ignited with probability  $q_{tk'}$ . This probability  $q_{tk'}$  depends on: (i) a reference probability that cell  $k'$  will be burning under no wind and flat terrain,  $q_{0k'}$ ; (ii) the vegetation type,  $q_{k'}^{\text{veg}}$ , and vegetation density,  $q_{k'}^{\text{den}}$ ; (iii) geographical information,  $q_{k'}^{\text{s}}$ ; and (iv) wind speed and direction,  $q_{tk'}^w$ , as follows:

$$q_{tk'} = q_{0k'} (1 + q_{k'}^{\text{veg}}) (1 + q_{k'}^{\text{den}}) q_{k'}^{\text{s}} q_{tk'}^w.$$

We refer to Ref. [22] and [37] for detailed parameter values.

*Probability of Fault  $p_{tc}$ :* Transmission lines are more prone to failures than other electrical components due to environmental factors such as lightning and wind [38]. Therefore, in our implementation, we focus on the fault at transmission lines and set  $p_{tc} = 0, \forall c \in \mathcal{B} \cup \mathcal{G}$ . This setup can be easily extended if we want to consider the risk of fault at buses and generators. In any time period, we assume a constant fault probability for each line  $l \in \mathcal{L}$  as  $p_{tl} = 1 - e^{-\bar{\lambda}}$ , where  $\bar{\lambda}$  is the estimated hourly failure rate in the Poisson regression model of [38].

#### C. Computational Performance and Solution Analysis

We examine how the algorithm performance and solution quality change with sample size. Our two-stage SMIP model,

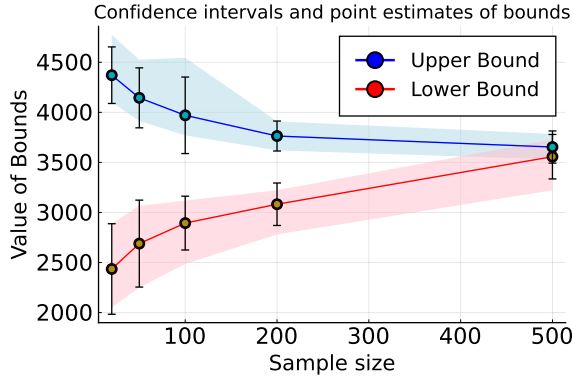


Fig. 5: Confidence intervals (bar) and point estimates (circle) of the lower and upper bounds for solutions with different sample sizes. The shaded area indicates the range of extreme values (maximum and minimum).

utilizing a set of scenarios  $\Omega$ , can be considered sample average approximation (SAA) and serve as a lower bound estimator of the optimal value for the true stochastic process of wildfire progression. As the number of scenarios increases, the approximation precision improves, but the required computational effort also increases [19]. Our objective is to determine a sample size that yields a high-quality solution within an acceptable computational budget. To achieve this, we first obtain twenty first-stage SAA solutions  $\hat{X} = \{\hat{x}, \hat{z}, \hat{\theta}, \hat{P}\}$  and optimal values with sample sizes of 20, 50, 100, 200, and 500.

Next, we generate  $n = 5,000$  wildfire scenarios  $\tilde{\Omega}$  using the procedure outlined in Section II-A for the out-of-sample test. We evaluate the expected total cost of each SAA solution using those 5,000 scenarios as follows:

$$g_n(\hat{X}) = \min_{\omega \in \tilde{\Omega}} \frac{1}{n} \left[ \sum_{t=1}^{\tau^{\omega}-1} \sum_{d \in \mathcal{D}} w_d(1 - \hat{x}_{dt}) + f^{\omega}(\hat{z}_{\cdot, \tau^{\omega}-1}, \xi^{\omega}) \right]. \quad (8)$$

Such cost can serve as an upper-bound estimator for the true wildfire progression. We take the mean of those twenty lower- and upper-bound estimators and calculate their 95% confidence intervals for each sample size, shown in Fig. 5. As the figure illustrates, the gap between the lower- and upper-bound estimators narrows, and both estimators become less variable with increasing sample size. We consider this gap acceptable for a sample size of 500.

As the sample size increases, solving the SMIP model (1) becomes significantly more challenging. As shown in Table I, Algorithm 1 with SMC, scales well and can solve the model with a sample size of 500 within a reasonable time (18,000 seconds). In contrast, state-of-the-art MIP solvers like Gurobi are unable to solve such a problem. The table also demonstrates that computational improvement by utilizing SMC is necessary, as the algorithm with original Lagrangian cuts (LC) cannot reach the optimum within the given time limit.

The nominal plan obtained by model (1) balances the trade-off between minimizing load-shedding cost and reducing wildfire risk. For example, transmission line 72 has a high risk of starting an endogenous wildfire, as it ranks 10-th among all

TABLE I: Run-time (sec.) of Algorithm 1 utilizing SMC and LC with a tolerance of 1.0%, compared with a run-time of solving model (1) by Gurobi with MIPGap = 1%.

Sample size	Algorithm 1 Time		Gurobi Time (Sec.)
	SMC (Sec.)	LC (Sec.)	
20	712	3287	84
50	1248	8741	376
100	2604	17911	1510
200	5323	> 18000	9186
500	12776	> 18000	> 18000

transmission lines regarding the number of scenarios where this occurs. However, the nominal plan does not de-energize it because it connects to a bus with multiple generators that supply a large amount of load; see Fig. 6a. To illustrate this trade-off, we compare the outcomes of de-energizing and keeping line 72 energized. If we *intentionally* de-energize line 72, it causes a significant loss of generation and load shed; see Fig. 6b. The load-shedding cost outweighs the expected damage cost caused by line 72, so the nominal plan prefers to keep it energized. However, after period 22, the nominal plan de-energizes it (Fig. 6c) because the expected damage cost from its fault exceeds the load-shedding cost from less generation. This decision is based on a 24 time-period horizon.

#### D. Benchmark Comparison

We choose the best optimal solution obtained from twenty batches with a sample size of 500 in Section IV-C as the solution to our two-stage SMIP model (1), denoted as  $X^* = \{x^*, z^*, \theta^*, P^*\}$ . We then compare this optimal solution,  $X^*$ , to the following three benchmark models:

- 1) A deterministic model where we maximize load satisfaction without considering possible disruption:

$$(M^{det}) \quad \min \quad \sum_{t=1}^T \sum_{d \in \mathcal{D}} w_d(1 - x_{dt})$$

s.t. Constraints (1a) – (1j).

Since  $(M^{det})$  does not consider the wildfire risk, the optimal solution will return a nominal plan  $X^{det} = \{x^{det}, z^{det}, \theta^{det}, P^{det}\}$  with no shut-off.

- 2) A wait-and-see model where we can make a scenario-specific plan assuming  $\xi^{\omega}$  is known before we make decisions. For each  $\omega \in \Omega$ , we solve

$$(M^{ws, \omega}) \quad g^{ws, \omega} = \min \quad \sum_{t=1}^{\tau^{\omega}-1} \sum_{d \in \mathcal{D}} w_d(1 - x_{dt}) + f^{\omega}(z_{\cdot, \tau^{\omega}-1}, \xi^{\omega})$$

s.t. Constraints (1a) – (1j),

and obtain a scenario-specific solution  $X^{ws, \omega} = \{x^{ws, \omega}, z^{ws, \omega}, \theta^{ws, \omega}, P^{ws, \omega}\}$ . An expected wait-and-see cost can then be computed as  $g_n^* = \sum_{\omega \in \Omega} g^{ws, \omega}$ .

- 3) A wildfire-risk-based model proposed by [18] to simultaneously reduce wildfire risk and load shedding:

$$(M^{rb}) \quad \min \quad \sum_{t=1}^T \left[ \frac{\alpha R_{Fire, t}}{R_{Tot}} - (1 - \alpha) \frac{\sum_{d \in \mathcal{D}} x_{dt} w_d D_{dt}}{D_{Tot}} \right]$$

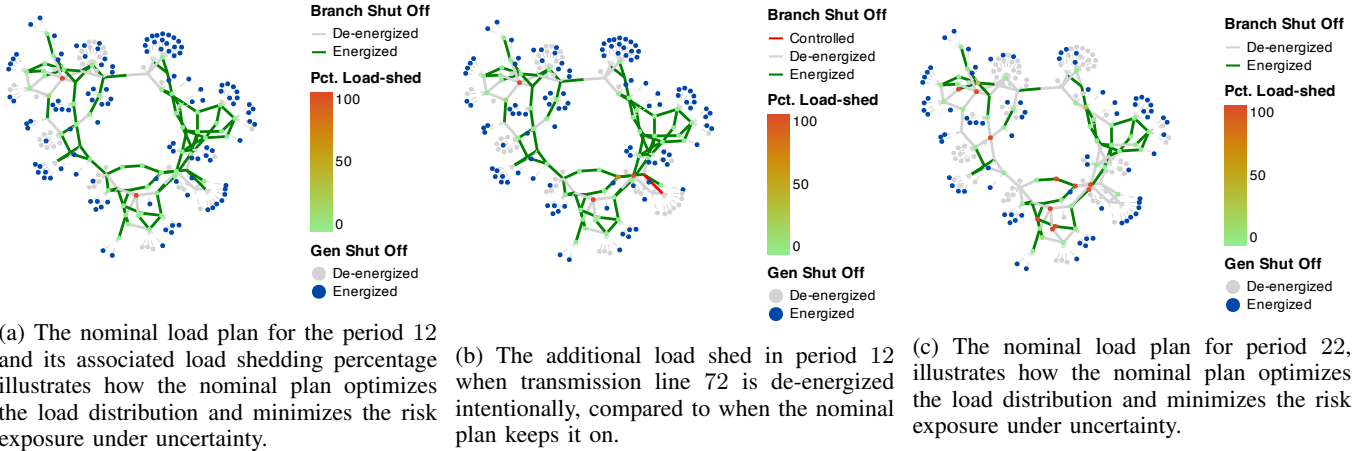


Fig. 6: Visualization of trade-off in the nominal plan. The red line in the bottom-right corner represents transmission line 72.

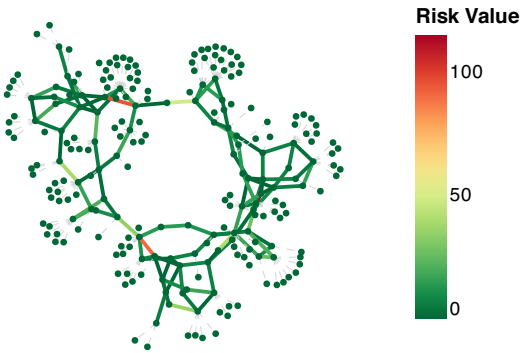


Fig. 7: Illustration of wildfire risk  $R_{ct}$  at  $t = 13$ .

$$\begin{aligned} \text{s.t.} \quad & \text{Constraints (1a) – (1j)} \\ & R_{Fire,t} = \sum_{c \in \mathcal{C}} R_{ct} z_{ct} \quad \forall t \in \mathcal{T}, \end{aligned}$$

The component-wise risk measure  $R_{ct}$  is the mean number of components affected by an endogenous fire started at component  $c$  across all scenarios. Fig. 7 illustrates the value of  $R_{ct}$  for  $t = 13$ . The components that face significant wildfire risk are marked in the figure. By controlling the number of energized components, we can compute the total wildfire risk  $R_{Fire,t}$  for the period  $t$ . We use the total load  $D_{Tot} = \sum_{d \in \mathcal{D}, t \in \mathcal{T}} D_{dt}$  and total wildfire risk  $R_{Tot} = \sum_{c \in \mathcal{C}, t \in \mathcal{T}} R_{ct}$  as the normalization factors such that we can combine the wildfire risk and the shed load in the objective function. The parameter  $\alpha \in [0, 1]$  adjusts the trade-off between serving loads and reducing wildfire risk. Solving model  $(M^{rb})$  returns a nominal plan  $X^{rb,\alpha} = \{x^{rb,\alpha}, z^{rb,\alpha}, \theta^{rb,\alpha}, P^{rb,\alpha}\}$ .

Each model is solved, then evaluated with the same  $n = 5,000$  out-of-sample scenarios  $\tilde{\Omega}$  used to evaluate the two-stage SMIP model (1). For the deterministic model and the wait-and-see model, we obtain two following ratios to show

their relative difference compared to model (1):

$$\frac{g_n(X^{det}) - g_n(X^*)}{g_n(X^*)} = 0.639 \quad \text{and} \quad \frac{g_n(X^*) - g_n^*}{g_n(X^*)} = 0.416.$$

The first ratio emphasizes that the two-stage SMIP can significantly improve the operations compared to the deterministic approach agnostic to potential wildfires. The second ratio quantifies the value of perfect information. We can save 41.6% of the cost if we can forecast the wildfire perfectly before we make the shut-off decisions. This large ratio reflects the high variance in wildfire scenarios and the difficulty for a single nominal shut-off plan to perform optimally in all scenarios. While it is not entirely possible to obtain the perfect information, it is helpful if we can obtain auxiliary data, conditioned on which we can identify a better representation of the scenarios. For example, we may exclude the scenarios with wildfires occurring in areas with forecast precipitation.

Fig. 8 illustrates such effect by selecting a subset of twenty scenarios: we can observe that the cost of the SMIP solution is significantly lower than the cost of the deterministic solution in all but one of the selected scenarios and can approach the best possible cost in two scenarios. If the auxiliary data happen to show those two scenarios are likely to happen, our SMIP solution will perform well. On the contrary, if the auxiliary data tell the other way, we may want to re-solve the two-stage SMIP model 1 with a refined set of scenarios.

For the wildfire-risk-based model  $(M^{rb})$ , we use the set of scenarios  $\Omega^*$ , with which we obtain  $X^*$ , to calculate the wildfire risk value  $R_{Fire,t}$  for all  $t \in \mathcal{T}$ . We obtain a solution  $X^{rb,\alpha}$  for  $\alpha \in \{0.0, 0.1, \dots, 0.9\}$ . We list the out-of-sample mean load-shedding cost and wildfire damage cost under non-disruptive scenarios (no wildfire ignitions) and disruptive scenarios in Table II, evaluated with  $\tilde{\Omega}$ .

If the wildfire risk is ignored ( $\alpha = 0.0$ ), it is equivalent to the deterministic solution  $X^{det}$ , which leads to a large out-of-sample cost  $g_n(X^{det})$ . By increasing  $\alpha$ , we can first reduce the total cost via the preventive shut-offs of potentially risky components, resulting in less damage cost. However, as  $\alpha$  increases further, the nominal plan becomes too conservative, and many components are de-energized such that the increas-

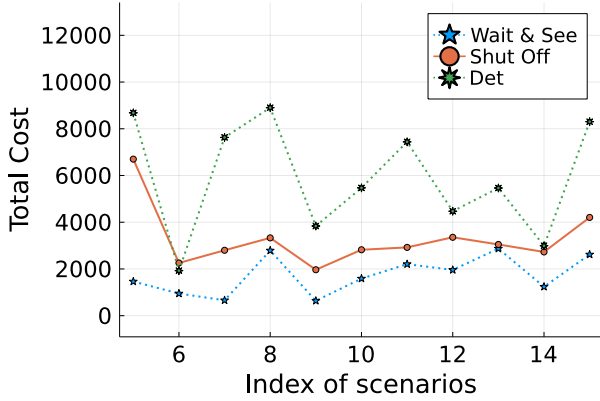


Fig. 8: Scenario-specific costs for model (1), the deterministic model ( $M^{det}$ ), and the wait-and-see model ( $M^{ws,\omega}$ ). For each scenario, the green star and orange circle represent the costs incurred by the nominal plans generated by ( $M^{det}$ ) and model (1). The blue star marks the wait-and-see cost.

ing load-shedding cost outweighs the reduced damage costs. This illustrates a major challenge in the wildfire-risk-based model ( $M^{rb}$ ) as there is little guidance to select a proper  $\alpha$ .

We then compare our SMIP model (1) with the wildfire-risk-based model ( $M^{rb}$ ), via the ratio of relative improvements (RRI)  $(g_n(X^{rb,\alpha}) - g_n(X^*)) / g_n(X^*)$  in Table II. The results show that the nominal plan obtained by solving model (1) performs significantly better. The reason is that ( $M^{rb}$ ) only considers minimizing the total wildfire risk and satisfying the power demand, which leads to the nominal plans that de-energize any component with  $R_{ct} > 0$  for some  $t \in \mathcal{T}$  as early as possible, only if this action does not affect the future supply of electricity. However, this property may compromise the resilience of the power grid by de-energizing an excessive number of components. If a disruption occurs, there might be very high load-shedding costs.

TABLE II: Load-shedding costs and damage costs of nominal plans  $X^{rb,\alpha}$  under non-disruptive and disruptive scenarios.

$\alpha$	Non-Disr.		Disruptive		Cumulation	
	Load shed	Load shed	Damage	$g_n(\cdot)$	RRI	
$0.0/X^{det}$	0.0	3247.0	2814.0	5936.2	63.9%	
0.1	148.6	3843.5	1767.5	5495.4	51.7%	
0.2	162.9	3850.7	1739.8	5480.8	51.4%	
0.3	221.4	3891.0	1713.9	5489.4	51.6%	
0.4	171.6	3786.3	1783.4	5454.9	50.6%	
0.5	251.1	3712.8	1773.9	5373.7	48.4%	
0.6	106.7	3686.8	1817.0	5390.5	48.9%	
0.7	469.3	3721.4	1754.1	5425.9	50.0%	
0.8	883.6	3949.0	1700.1	5532.7	52.8%	
0.9	1505.8	4285.3	1341.1	5510.5	52.2%	

### E. Sensitivity Analysis of Disruption Probability

We simulate the set of wildfire scenarios with a probabilistic model described in Section II-A and IV-B, which then serves as the uncertainty model in the SMIP. It is necessary to examine the robustness of the optimal solution to the SMIP against the potential inaccuracy in such an uncertainty model.

Therefore, we perform a sensitivity analysis in this section to check the out-of-sample performance of SMIP solutions obtained with different uncertainty assumptions.

In Section II, we construct a scenario set  $\Omega^*$  in the SMIP model (1), each scenario with an equal probability of occurrence,  $1/|\Omega^*|$ . Such a scenario set can be partitioned as  $\Omega^* = \Omega_D^* \cup \Omega_N^*$ , where  $\Omega_D^*$  ( $\Omega_N^*$ ) represents the set of scenarios with(out) a disruption. When there is no disruption, the nominal plan is carried out over the entire time horizon. Therefore, the partition is equivalent to  $\Omega^* = \Omega_D^* \cup \{\omega_0\}$  with probabilities  $p^{\omega_0} = |\Omega_N^*|/|\Omega^*|$  and  $p^\omega = (1 - p^{\omega_0})/|\Omega_D^*|$  for  $\omega \in \Omega_D^*$ , where  $\omega_0$  is a scenario without disruption.

For the sensitivity analysis, we add a perturbation  $\Delta p$  to  $p^{\omega_0}$  and adjust  $p^\omega$  for  $\omega \in \Omega_D^*$  accordingly. We solve the SMIP for each  $\Delta p$  and test its solution's out-of-sample performance over the scenario set  $\tilde{\Omega}$ , displayed in Table III. The out-of-sample no-disruption probability  $|\tilde{\Omega}_N|/|\tilde{\Omega}|$  is approximately 0.05, similar to that of  $\Omega^*$ .

We observe from Table III that the optimal SMIP solution can yield a decent out-of-sample performance even when the input perturbation is quadruple the original no-disruption probability ( $\Delta p = 0.2$ ). This indicates that the SMIP optimal solution is robust against input inaccuracy. When  $\Delta p$  keeps increasing, the SMIP values a nominal plan that shuts off fewer components and thus minimizes the load shed under scenarios without wildfire disruption. It leads to higher out-of-sample load-shedding and damage costs simultaneously as insufficient shut-offs are executed to prevent endogenous wildfires. The sensitivity analysis results show that the SMIP optimal solution is reliable as long as the input uncertainty model is not too liberal when estimating the wildfire risk.

TABLE III: Load-shedding costs and damage costs of nominal plans  $X^{\Delta p}$  under non-disruptive and disruptive scenarios.

$\Delta p$	Non-Disr.		Disruptive		Cumulation	
	Load shed	Load shed	Damage	$g_n(\cdot)$	RRI	
-0.05	1805.1	2553.0	1242.7	3782.8	4.5%	
-0.015	1741.5	2513.7	1353.6	3787.3	4.6%	
$0.0/X^*$	1678.2	2355.2	1333.6	3612.7	0.0%	
0.015	1660.0	2343.9	1341.7	3609.7	-0.1%	
0.05	1504.9	2360.2	1325.4	3609.6	-0.1%	
0.1	1250.7	2344.8	1317.1	3586.5	-0.7%	
0.2	828.4	2196.5	1578.8	3697.5	2.3%	
0.3	207.3	2181.1	1752.3	3882.5	7.3%	
0.5	185.1	2343.5	1845.6	4109.1	13.5%	
0.7	109.7	2410.8	1851.0	4153.3	15.0%	
0.9	99.0	2476.8	1878.1	4276.7	18.4%	

## V. CONCLUSIONS & FUTURE WORK

This work contributes to the literature on stochastic optimization for power system operation under wildfire risk. We propose a novel two-stage stochastic program that captures the uncertainty of wildfire disruptions and temporal dynamics. We also develop an efficient decomposition algorithm that exploits the binary structure of state variables and generates valid cuts for solving large-scale instances. Our numerical experiments demonstrate the effectiveness and robustness of our approach in terms of solution quality and computational speed. They

illustrate the benefits of the stochastic programming model by comparing it with deterministic counterparts.

For future work, we plan to extend our research in several directions. One direction is to investigate a theory-driven approach for generating effective and efficient cuts in our decomposition algorithm. Another direction is to relax the assumption of at most one disruption and extend our model as a multistage problem, which can still be solved by our algorithm due to the binary nature of state variables. A third direction is to address the challenge of ensuring feasibility with AC power flow when using a linear approximation of power flow in our model. Finally, we aim to develop a rolling horizon framework that can handle the wildfire forecast updates and dynamically re-optimize the de-energization schedule.

## REFERENCES

- [1] J. W. Muhs, M. Parvania, and M. Shahidehpour, "Wildfire risk mitigation: A paradigm shift in power systems planning and operation," *IEEE Open Access Journal of Power and Energy*, vol. 7, pp. 366–375, 2020.
- [2] T. P. Holmes, R. J. Huggett Jr, and A. L. Westerling, "Statistical analysis of large wildfires," *The Economics of Forest Disturbances*, vol. 79, pp. 59–77, 2008.
- [3] B. Teague, R. Mcleod, and S. Pascoe, "Final report: 2009 Victorian Bushfires Royal Commission," Victorian Bushfires Royal Commission, Tech. Rep. 332, 2010.
- [4] "2019 wildfire risk report," CoreLogic, Tech. Rep., 2019. [Online]. Available: [https://www.corelogic.com/wp-content/uploads/sites/4/downloadable-docs/wildfire-report\\_0919-01-screen.pdf](https://www.corelogic.com/wp-content/uploads/sites/4/downloadable-docs/wildfire-report_0919-01-screen.pdf)
- [5] B. Evarts, "Fire loss in the United States during 2018," National Fire Protection Association, Tech. Rep., 2019.
- [6] S. Li and T. Banerjee, "Spatial and temporal pattern of wildfires in California from 2000 to 2019," *Scientific Reports*, vol. 11, no. 1:8779, 2021.
- [7] N. Rhodes, L. Ntaimo, and L. Roald, "Balancing wildfire risk and power outages through optimized power shut-offs," *IEEE Transactions on Power Systems*, vol. 36, no. 4, pp. 3118–3128, 2021.
- [8] J. H. Scott, M. P. Thompson, and D. E. Calkin, "A wildfire risk assessment framework for land and resource management," U.S. Department of Agriculture, Forest Service, Rocky Mountain Research Station, Tech. Rep. RMRS-GTR-315, 2013.
- [9] S. Dian, P. Cheng, Q. Ye, J. Wu, R. Luo, C. Wang, D. Hui, N. Zhou, D. Zou, Q. Yu, and X. Gong, "Integrating wildfires propagation prediction into early warning of electrical transmission line outages," *IEEE Access*, vol. 7, pp. 27 586–27 603, 2019.
- [10] S. Jazebi, F. de León, and A. Nelson, "Review of wildfire management techniques—Part I: Causes, prevention, detection, suppression, and data analytics," *IEEE Transactions on Power Delivery*, vol. 35, no. 1, pp. 430–439, 2020.
- [11] Pacific Gas and Electric Company, "PG&E announces major new electric infrastructure safety initiative to protect communities from wildfire threat," 2021. [Online]. Available: <https://tinyurl.com/5edcaxmx>
- [12] "Utility public safety power shutoff plans (de-energization)." California Public Utilities Commission (CPUC), 2022. [Online]. Available: <https://www.cpuc.ca.gov/psps/>
- [13] *Pacific Gas and Electric Company Amended 2019 Wildfire Safety Plan*, Pacific Gas and Electric Company, 2019. [Online]. Available: <https://tinyurl.com/nhcepspp>
- [14] S. Jazebi, F. de León, and A. Nelson, "Review of wildfire management techniques—Part II: Urgent call for investment in research and development of preventative solutions," *IEEE Transactions on Power Delivery*, vol. 35, no. 1, pp. 440–450, 2020.
- [15] T. Zhou, B. Li, C. Wu, Y. Tan, L. Mao, and W. Wu, "Studies on big data mining techniques in wildfire prevention for power system," in *2019 IEEE 3rd Conference on Energy Internet and Energy System Integration (EI2)*, 2019, pp. 866–871.
- [16] W. Hong, B. Wang, M. Yao, D. Callaway, L. Dale, and C. Huang, "Data-driven power system optimal decision making strategy under wildfire events," Lawrence Livermore National Lab, Tech. Rep. LLNL-CONF-831390, 2022.
- [17] A. Lesage-Landry, F. Pellerin, J. A. Taylor, and D. S. Callaway, "Optimally scheduling public safety power shutoffs," *arXiv preprint arXiv:2203.02861*, 2022.
- [18] N. Rhodes and L. Roald, "Co-optimization of power line de-energization and restoration under high wildfire ignition risk," *arXiv preprint arXiv:2204.02507*, 2022.
- [19] J. R. Birge and F. Louveaux, *Introduction to Stochastic Programming*. New York, NY, USA: Springer-Verlag, 1997.
- [20] H. Yang and H. Nagarajan, "Optimal power flow in distribution networks under N-1 disruptions: A multistage stochastic programming approach," *INFORMS Journal on Computing*, vol. 34, no. 2, pp. 690–709, 2022.
- [21] J. Zou, S. Ahmed, and X. A. Sun, "Stochastic dual dynamic integer programming," *Mathematical Programming*, vol. 175, no. 1-2, pp. 461–502, 2019.
- [22] J. Freire and C. Dacamara, "Using cellular automata to simulate wildfire propagation and to assist in fire prevention and fighting," *Natural Hazards and Earth System Sciences Discussions*, pp. 1–17, 2018.
- [23] C. Lemaréchal, A. Nemirovskii, and Y. Nesterov, "New variants of bundle methods," *Mathematical programming*, vol. 69, no. 1, pp. 111–147, 1995.
- [24] C. Barrows, A. Bloom, A. Ehlen, J. Ikäheimo, J. Jorgenson, D. Krishnamurthy, J. Lau, B. McBenett, M. O'Connell, E. Preston, A. Staid, G. Stephen, and J.-P. Watson, "The IEEE reliability test system: A proposed 2019 update," *IEEE Transactions on Power Systems*, vol. 35, no. 1, pp. 119–127, 2020.
- [25] "Texas A&M forest service: Texas wildfire risk assessment portal." [Online]. Available: <https://texaswildfirerisk.com/>
- [26] World Nuclear Association, "Economics of nuclear power," 2022. [Online]. Available: <https://world-nuclear.org/information-library/economic-aspects/economics-of-nuclear-power.aspx>
- [27] D. Blewett, "Wind turbine cost: How Much? Are They Worth It In 2022?" 2022. [Online]. Available: <https://weatherguardwind.com/how-much-does-wind-turbine-cost-worth-it/>
- [28] World Nuclear Association, "Financing nuclear energy," 2020. [Online]. Available: <https://world-nuclear.org/information-library/economic-aspects/financing-nuclear-energy.aspx>
- [29] "2021 transmission cost report." Australian Energy Market Operator, Tech. Rep., 2021. [Online]. Available: <https://aemo.com.au/-/media/files/major-publications/isp/2021/transmission-cost-report.pdf?la=en>
- [30] I. Dunning, J. Huchette, and M. Lubin, "JuMP: A modeling language for mathematical optimization," *SIAM Review*, vol. 59, no. 2, pp. 295–320, 2017.
- [31] S. K. Jeff Bezanson, Alan Edelman and V. Shah, "Julia: A fresh approach to numerical computing," *SIAM Review*, 2014.
- [32] Gurobi Optimization, Inc., *Gurobi optimizer reference manual.*, 2014. [Online]. Available: <https://www.gurobi.com>
- [33] C. Coffrin, R. Bent, K. Sundar, Y. Ng, and M. Lubin, "Powermodels.jl: An open-source framework for exploring power flow formulations," in *2018 Power Systems Computation Conference (PSCC)*, June 2018, pp. 1–8.
- [34] G. Datseris, A. R. Vahdati, and T. C. DuBois, "Agents.jl: a performant and feature-full agent-based modeling software of minimal code complexity," *Simulation*, p. 003754972110688, 2022.
- [35] MapTools, "Why use UTM coordinates," 2023. [Online]. Available: [https://www.maptools.com/tutorials/utm/why\\_use\\_utm](https://www.maptools.com/tutorials/utm/why_use_utm)
- [36] "Wildland fire potential index (WFPI)." [Online]. Available: <https://www.usgs.gov/fire-danger-forecast/wildland-fire-potential-index-wfpi>
- [37] A. Alexandridis, D. Vakalis, C. Siettos, and G. Bafas, "A cellular automata model for forest fire spread prediction: The case of the wildfire that swept through Spetses island in 1990," *Applied Mathematics and Computation*, vol. 204, no. 1, pp. 191–201, 2008.
- [38] S. Yang, W. Zhou, S. Zhu, L. Wang, L. Ye, X. Xia, and H. Li, "Failure probability estimation of overhead transmission lines considering the spatial and temporal variation in severe weather," *Journal of Modern Power Systems and Clean Energy*, vol. 7, no. 1, pp. 131–138, 2019.